PHYSICAL REVIEW B **94**, 241106(R) (2016)

Mass inversion in graphene by proximity to dichalcogenide monolayer

Abdulrhman M. Alsharari,[1,2,*] Mahmoud M. Asmar,[3] and Sergio E. Ulloa[1]

[1]*Department of Physics and Astronomy, Nanoscale and Quantum Phenomena Institute, Ohio University, Athens, Ohio 45701, USA*

[2]*Department of Physics, University of Tabuk, Tabuk 71491, Saudi Arabia*

[3]*Department of Physics and Astronomy, Louisiana State University, Baton Rouge, Louisiana 70803, USA*

(Received 2 August 2016; revised manuscript received 23 September 2016; published 13 December 2016)

Proximity effects resulting from depositing a graphene layer on a transition-metal dichalcogenide substrate layer change the dynamics of the electronic states in graphene, inducing spin-orbit coupling and staggered potential effects. An effective Hamiltonian that describes different symmetry-breaking terms in graphene, while preserving time-reversal invariance, shows that an inverted mass band-gap regime is possible. The competition of different perturbation terms causes a transition from an inverted mass phase to a staggered gap in the bilayer heterostructure as seen in its phase diagram. A tight-binding calculation of the bilayer validates the effective model parameters. A relative gate voltage between the layers may produce such a phase transition in experimentally accessible systems. The phases are characterized in terms of Berry curvature and valley Chern numbers, demonstrating that the system may exhibit quantum spin Hall and valley Hall effects.

DOI: 10.1103/PhysRevB.94.241106

1. Introduction. Graphene has many interesting properties intensively studied in recent years [1]. Prominent among these, possible intrinsic spin-orbit coupling (SOC) on its charge carriers was estimated by Kane and Mele to be rather weak $\simeq 1\,\mu$eV [2]. Improved estimates that include contributions from d orbitals yield larger values of $\simeq 24\,\mu$eV [3], although still rather weak for experimental observation. Several ways have been proposed to enhance SOC in graphene for uses in spintronics [4]. Enhancing sp^3 hybridization by adding hydrogen or fluorene atoms [5] as well as decorating with heavy adatoms [6] or different substrates [7] has been proposed to produce large SOC. Depositing graphene on metallic substrates also has resulted in strong SOC [8].

The availability of two-dimensional (2D) crystals allows for novel stacked heterostructures with strong proximity effects. Electronic modulation due to such substrates has been studied in graphene, such as hexagonal boron nitride (hBN) or twisting of another graphene layer [9–16]. Lattice commensurability in these heterostructures depends on factors, such as isotropic expansion, relative sliding between layers, and relative twists [13,17,18].

An interesting family of 2D crystals, transition-metal dichalcogenides (TMD) can be used as substrates for graphene [19–23]. Monolayer semiconductor TMDs, such as MoS_2 and WS_2 have a direct band gap and honeycomb crystal structure [24]. The bands near the Fermi energy are formed predominantly from d orbitals of the metal atom [25] with a slight admixture from the p orbitals of the chalcogen. The SOC in the valence bands is much larger than in the conduction bands with a strength that varies with the transition metal [26]. Successful growth of graphene on MoS_2 and WS_2 has been demonstrated experimentally [22,27–30]. First-principles calculations on some of these systems have proved challenging [21–23] with reported results that differ qualitatively and quantitatively.

Motivated by these works, we study the topological properties of the minimal time-reversal invariant effective model of graphene that incorporates geometrical and orbital perturbation effects expected in these systems. Although the effective Hamiltonian of the system can be obtained by a variety of methods [21,22], its topological phases remain unexplored. We focus on the Berry curvature and associated valley Chern number and identify different quantum phases that may appear as Hamiltonian parameters vary. The phase diagram shows that, under the right conditions, it is possible to achieve band inversion of spin-split bands in graphene that acquire interesting characteristics from the proximal TMD layer. We further identify that a relative voltage difference between the graphene and the TMD layer (as obtained by an applied external field) can drive a transition between two topologically inequivalent phases, separated by a semimetallic phase.

The reduction of the spatial symmetries of graphene and the enhancement of SOC in these systems result in the generation of spin-resolved gaps at the Dirac point. The interplay between sublattice symmetry breaking and enhanced SOC parameters determines the size and topological nature of the gaps in the system. As the gaps are dominated by SOC, the system becomes a quantum spin Hall insulator with symmetry-protected edge states. In contrast, when the gaps are dominated by the sublattice staggered symmetry, the system becomes a valley Hall insulator.

Identification of experimentally relevant parameters is carried out utilizing a tight-binding calculation with appropriate graphene and TMD characteristics. Different lattice orientations and relative layer displacement also are found to exhibit such a phase transition with shifts in the values of the external field at which it occurs.

2. Effective model and characteristics. The proximity of the TMD monolayer to graphene breaks inversion symmetry, which allows for the presence of Rashba SOC in addition to sublattice asymmetry terms in the effective Hamiltonian [31]. A minimal low-energy model will include terms that respect time-reversal symmetry [23,32] and arise due to the

*aalsharari@ut.edu.sa

symmetries in the TMD states $\mathcal{H}_{\rm eff} = \mathcal{H}_0 + \mathcal{H}_\Delta + \mathcal{H}_{S_1} + \mathcal{H}_{S_2} + \mathcal{H}_R$ with

$$\begin{aligned} \mathcal{H}_0 &= \hbar v_F(\tau_z\sigma_x s_0 p_x + \tau_0\sigma_y s_0 p_y), \\ \mathcal{H}_\Delta &= \Delta s_0\sigma_z\tau_0, \\ \mathcal{H}_{S_1} &= S_1\tau_z\sigma_z s_z, \\ \mathcal{H}_{S_2} &= S_2\tau_z\sigma_0 s_z, \\ \mathcal{H}_R &= R(\tau_z\sigma_x s_y - \tau_0\sigma_y s_x), \end{aligned} \tag{1}$$

where σ_i, τ_i, and s_i are 2×2 Pauli matrices with $i = 0,x,y,z$, (0 is for the unit matrix) operating on different degrees of freedom. σ_i acts on the pseudospin sublattice space (A,B), τ_i on the K,K' valley space, and s_i on the spin [31]. We use the "standard" basis $\Psi^T = (\Psi_K^T, \Psi_{K'}^T)$ with $\Psi_{K,K'}^T = (A\uparrow, B\uparrow, A\downarrow, B\downarrow)_{K,K'}$, and $\mathcal{H}_0$ describes pristine graphene [2]. The parameters v_F, Δ, S_1, S_2, and R are constants of the model, to be obtained from density functional theory or tight-binding calculations (as we describe below). They would naturally be expected to depend on the microscopic details of the system, such as orientation and relative displacements of the monolayers, as well as on applied electric fields or pressure. As we will see below, it is such a dependence that may give rise to interesting phases.

$\mathcal{H}_\Delta$ characterizes the (staggered) sublattice asymmetry in the graphene A and B atoms as expected from proximity to the TMD monolayer; this term is well known to open gaps in the otherwise linear dispersion of $\mathcal{H}_0$ and create sizable topological-valley currents in graphene-hBN superlattices [16,32]. The intrinsic SOC term $\mathcal{H}_{S_1}$ opens a spin gap in the bulk structure with opposite signs at K,K' valleys while preserving spatial symmetries of the hexagonal lattice. Finally, as mirror symmetry ($z \to -z$) is broken by the TMD substrate, the dynamics is expected to contain a Rashba effective Hamiltonian $\mathcal{H}_R$ [2] and a diagonal SOC term $\mathcal{H}_{S_2}$. Although a valley mixing term is possible in principle, we find it to be essentially null in all our calculations.

Typical band structures for this Hamiltonian are shown in Fig. 1. The left panel illustrates an inverted band regime, evident in the local dispersion around each of the valleys near the graphene neutrality point, produced by the anticrossing of bands with opposite spins and due to the presence of the Rashba term. The middle panel shows a transition point where the gap has closed and exhibits a dispersion with nearly full spin polarization. The right panel shows a direct band regime with a simple parabolic dispersion for each of the two spin projections. As we will see below, the inverted band regime is achieved whenever $|S_1 + S_2| > \Delta$, whereas the direct band regime is achieved in the opposite case.

One can analyze the topological features of the system by calculating the Berry curvature $\Omega_n(\boldsymbol{k})$ and Chern number per valley of the occupied bands using [33]

$$\begin{aligned} \Omega_n(\boldsymbol{k}) &= -\sum_{n'\neq n} \frac{2\,\mathrm{Im}\langle\Psi_{n'\boldsymbol{k}}|v_x|\Psi_{n\boldsymbol{k}}\rangle\langle\Psi_{n\boldsymbol{k}}|v_y|\Psi_{n'\boldsymbol{k}}\rangle}{(\epsilon_n - \epsilon_{n'})^2}, \\ \mathcal{C}_n &= \frac{1}{2\pi}\int dk_x dk_y \Omega_n(k_x,k_y), \end{aligned} \tag{2}$$

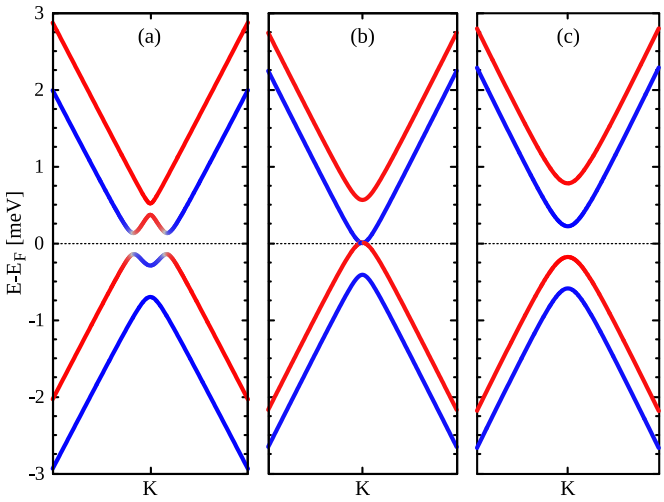

FIG. 1. Typical band structure of an effective model near the K valley. The left panel shows an "inverted band" regime with strong spin mixing of the different states as indicated by the red/blue shading and typical of $|S_1 + S_2| > \Delta$. The middle panel shows a spin-split semimetallic phase, whereas the right panel shows a "direct band" regime where a finite bulk gap develops with nearly full spin polarization, obtained when $|S_1 + S_2| < \Delta$.

where n is the band number and $v_x(v_y)$ is the velocity operator along the $x(y)$ direction [34]. Figure 2 shows Berry curvature for the two lowest-energy (valence) bands and total curvature near each of the K,K' valleys in two different parameter regimes. Notice plots for each band obey $\Omega(K\text{ valley}) = -\Omega(K'\text{ valley})$ as required by time-reversal symmetry [33]. The left two columns in Fig. 2, for the inverted band regime, exhibit a nonmonotonic k dependence for the curvature in each valley with inversion at each K point $\Omega_1(0) \simeq -\Omega_2(0)$

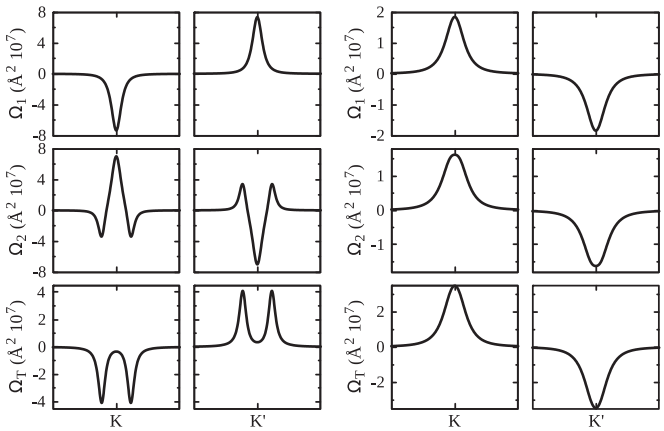

FIG. 2. Berry curvature Ω_n at K and K' valleys for both inverted and direct band-gap regimes. The left two columns show results for the inverted band regime corresponding to Fig. 1(a). The right two columns are for the direct band regime corresponding to Fig. 1(c). The upper (middle) plots describe Berry curvature of the lowest-(highest-) energy valence bands in Fig. 1, $n = 1(2)$. The lower plots show the total valence-band Berry curvature $\Omega_T = \Omega_1 + \Omega_2$. The different Berry curvature distributions between K and K' are evident in both cases.

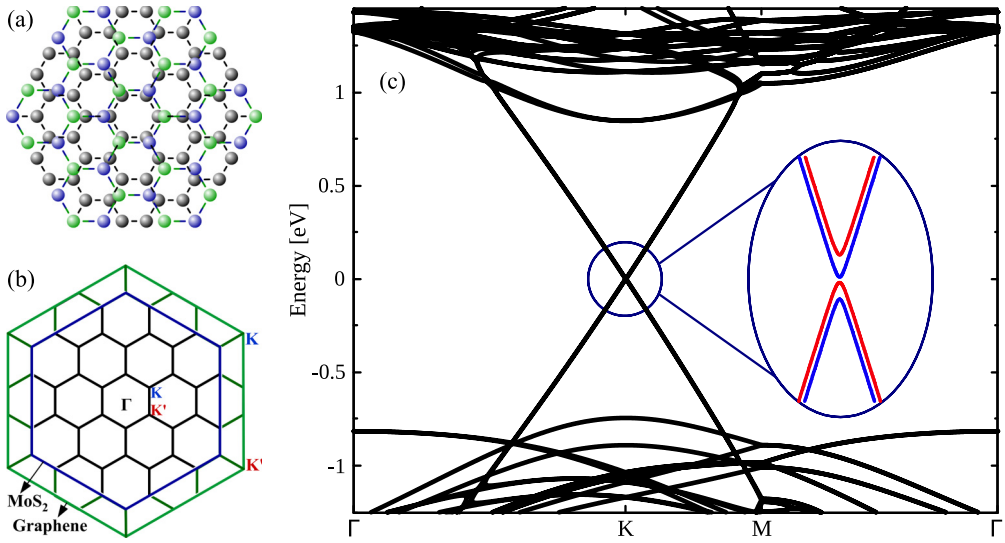

FIG. 3. Graphene-MoS_2 heterostructure. (a) Top view of bilayer structure supercell in real space. The black circles are A and B atoms of graphene, whereas blue (green) are Mo (S_2) atoms. (b) Brillouin zones of the reciprocal lattices: First BZ for a monolayer of graphene and MoS_2 with the positions of the K and K' valleys. Upon folding onto the heterostructure reciprocal lattice, corner valleys from both layers are mapped onto the same point. (c) Band dispersion of graphene-MoS_2 along high-symmetry lines Γ-K-M-Γ. The inset: Zoom near the K valley shows graphene bands appear gapped and spin polarized due to proximity to MoS_2. The blue (red) bands are for spin-up (spin-down) states.

so that the total valley curvature is nearly null. In contrast, the right two columns for the direct band regime show the same curvature for both bands in each valley. The nonvanishing Berry curvature in each valley may give rise to interesting edge states in systems with borders as seen in graphene ribbons and TMD flake edges [35–37].

The total Chern index at each valley yields $\mathcal{C}_K = -\mathcal{C}_{K'}$ for all parameter values so that the overall Chern number vanishes as expected for systems protected by time-reversal symmetry [33,38]. However, the spin splitting and mixing of the two valence bands in different regimes results in $\mathcal{C}_K = \pm 1$ with an overall sign change across the semimetallic phase transition where the gap closes. In a system with a zero Rashba term ($R = 0$), the Chern number can be shown to yield $\mathcal{C} = \mathrm{sgn}(\Delta\tau_z + S_1 s_z)$, indicating the competition between the intrinsic SOC and the staggered perturbations. Although an analytic expression for the Chern number is not feasible in general, numerical evaluation for different parameter regimes reveals the important roles of both S_1 and S_2 as well as R on determining the topological features of the system. We will return to this point in detail below.

3. Tight-binding model. The relevant effective model dependence on microscopic details of the graphene-TMD heterostructure can be obtained from a tight-binding model of the structure. We focus on graphene and MoS_2 with lattice constants 2.46 and 3.11 Å, respectively. A superlattice of 5×5 graphene and 4×4 MoS_2 unit cells results in a nearly commensurate moiré pattern with a small residual strain ($\sim$1.1%) as seen in Fig. 3(a). The corresponding Brillouin zone (BZ) has similar features to that of graphene with valleys at $\mathbf{K},\mathbf{K}' = \frac{2\pi}{a_\alpha}(\frac{1}{\sqrt{3}}, \pm\frac{1}{3})$, $a_\alpha = 5a_G = 4a_{\mathrm{Mo}}$, folding the valleys of graphene and MoS_2 onto the same points; see Fig. 3(b) as well as details in the Supplemental Material [39].

The tight-binding couples nearest-neighbors $\langle ij\rangle$ in an optimal basis where MoS_2 is represented by three orbitals d_{z^2}, d_{xy}, and $d_{x^2-y^2}$ [25],

$$\mathcal{H}_{\mathrm{Mo}} = \sum_{ivs} \epsilon_{vs} \alpha^\dagger_{ivs} \alpha_{ivs} + \sum_{\langle ij\rangle v\mu s} t_{iv,j\mu} \alpha^\dagger_{ivs} \alpha_{j\mu s} + \mathrm{H.c.} \quad (3)$$

ϵ_{vs} considers the on-site energies of Mo-atom i, orbital v, and spin s, whereas $t_{iv,j\mu}$ describes hopping between Mo orbitals. The SOC in MoS_2 is introduced via atomic contributions [25]. For graphene we adopt the usual p_z-orbital representation with a two-atom basis [1,39]. The substrate generates an electric field normal to the layer, causing a Rashba SOC term [2] $\mathcal{H}_R = i t_R \sum_{\langle ij\rangle \alpha\beta} \hat{z} \cdot (\mathbf{s}_{\alpha\beta} \times \mathbf{d}^\circ_{ij}) c^\dagger_{i\alpha} c_{j\beta}$, where α,β describe spin-up and spin-down states and $\mathbf{d}^\circ_{ij}$ is the unit vector that connects neighbor atoms A and B. Although the Rashba interaction is weak in graphene ($t_R = 0.067$ meV [40]), it is an important term that breaks inversion symmetry.

The interlayer coupling between the graphene p_z orbital and the MoS_2 d orbitals is given by

$$\mathcal{H} = \sum_{\langle ij\rangle, v\sigma} t^v_{i,j} c^\dagger_{i,\sigma} \alpha_{jv,\sigma} + \mathrm{H.c.} \quad (4)$$

The parameters used are described in Ref. [39], although the detailed values do not affect the main conclusions nor qualitative behavior, providing only an overall scaling.

The tight-binding model considers the possibility of a difference in electronegativity between the two layered materials creating a relative shift of their neutrality points. This polarization shift could be thought to arise from an effective potential difference across the layers as would be possible to apply if the graphene-MoS_2 structure is placed between capacitor plates. We explore the consequences of such relative voltage on the effective band structure on graphene, assuming that the other parameters (hopping integrals and lattice constants) remain unchanged with voltage. One could obtain the appropriate parameters from first-principles cal-

culations, although the van der Waals nature of the bonding between layers as well as the rather fine scale of the relevant features make those calculations quite challenging [21,22]. Results for a nearly zero relative shift of the neutrality points are in Fig. 3(c), which show how the low-energy spectrum exhibits a finite gap for fully spin-polarized bands. This band alignment agrees well with recent experiments in such a bilayer system [29].

As the relative voltage between layers is varied, the tight-binding spectrum shows a low-energy band structure similar to that of the effective model, Fig. 1. We have carried out a systematic fit of the low-energy dispersion with the model parameters in Eq. (1) as the voltage changes. The fits are excellent (to less than 1%) up to an energy 0.3 eV away from the graphene Dirac point with nearly linear dispersion at higher energies [29]. The effective model describes not only the low-energy band dispersion, but also the full spin and pseudospin structures of the states, illustrating the generality of the model [39]. Fit parameters vary smoothly with gate voltage as shown in Fig. 4(b); we assign $V_{\text{Gate}} = 0$ when the graphene Dirac point is 20 meV higher than the top valence band in MoS_2, whereas a zero relative shift of their neutrality points is at $V_{\text{Gate}} \simeq 0.9$ eV. The staggered potential Δ increases smoothly with voltage, whereas R, S_1, and S_2 vary much less [41]. Most importantly, we see that the gap closes near the gate voltage where the sum $\Delta + S_1 + S_2 + R/3 \simeq 0$. Figures 4(a) and 4(b) also show the valley Chern number jumps by 2π at the closing of the gap as anticipated from the discussion above, although here the competition involves Δ and all three SOC coefficients. We emphasize that the closing of the gap and corresponding phase transition from an inverted mass to a direct gap regime is rather generic and, as suggested by these calculations, accessible experimentally [42].

Notice that the model studied is one particular example of a large class of Hamiltonians that describe systems that possess similar symmetry properties with different parameters. More examples are graphene and other TMD heterostructures. In graphene-WS_2, the inverted band phase exists over a wider range of gate voltage with the gap closing at $V_{\text{Gate}} = 1.2$ eV. This larger voltage can be understood as arising from the larger SOC in WS_2, nearly three times stronger than in MoS_2 [24]. We also explored structures with a relative shift of the lattices or possible rotations of the two layers involved [39]. We find that gaps open generically near the graphene neutrality point with regimes of inverted masses at times over only narrow regions of gate voltage. This suggests that, in a macroscopic sample with a distribution of strains, one may expect variation of the effective Hamiltonian parameters over long-range scales. This may produce edge states separating different regions in the 2D bulk with different topological features, resulting in interesting effects even away from the sample edges [39].

The topology of the inverted mass regime in the structure suggests that edge states would exist at boundaries as discussed in the past [33]. In fact, zigzag edge graphene nanoribbons based on the effective Hamiltonian show different regimes. A quantum spin Hall effect is seen for the mass inverted bands, whereas a valley Hall effect is present in the direct band regime.

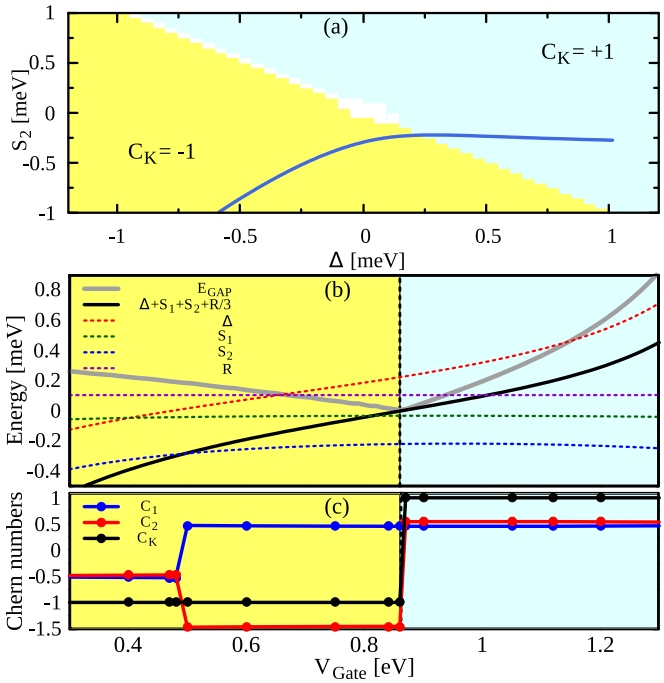

FIG. 4. (a) Phase diagram for the graphene-TMD system in Eq. (1) in the S_2-Δ projection with $R = 0.1$ meV and $S_1 \in [-0.16, 0.16]$ meV. The trivial insulating phase in blue $C_K = 1$ and the mass inverted phase in yellow $C_K = -1$, divided by the semimetallic phase, white curve. The blue line shows the line cut for the graphene-MoS_2 system as a function of V_{Gate}. (b) Gate voltage dependence of effective Hamiltonian parameters used to fit the tight-binding band-structure results. The black line shows evolution of the band gap, which closes at $V_{\text{Gate}} = 0.86$ eV. For $V_{\text{Gate}} = 0.86$ eV, in the inverted band regime, spin-orbit contribution dominates over the staggered term, given approximately by $\Delta + S_1 + S_2 < 0$, slightly shifted by the Rashba term. In the opposite regime, staggered potential dominates and creates a trivial band gap. (c) Chern numbers for the K valley as in (a). The switch near $V_{\text{Gate}} = 0.5$ eV is due to a band crossing at the K point, whereas the jump at $V_{\text{Gate}} = 0.86$ eV indicates a gap closing that separates the inverted mass regime from the direct band regime. $V_{\text{Gate}} = 0$ corresponds to a graphene Dirac point 20 meV higher than the top valence band in MoS_2.

4. Conclusions. We have built and studied a heterostructure of graphene deposited on a monolayer of TMDs in order to explore proximity effects. An effective Hamiltonian with perturbations that preserve time reversal is able to faithfully reproduce the results from tight-binding calculations of the structure near the graphene Dirac points. The TMD proximity results in sizable spin-orbit coupling imparted onto graphene in a degree proportional to the intrinsic SOC in the TMD. This strong effect is found to compete with the staggered potential also introduced, resulting in different regimes where the heterostructure changes phase from an inverted mass band structure with a possible quantum spin Hall effect and the consequent spin filtered edge states to a direct band structure with a possible valley Hall effect and the appearance of valley currents. These phases could in principle be controlled by an effective potential difference between the layers and may even be present throughout the 2D bulk as strain fields would affect the relevant phases present. Experimental

identification and optimization of parameters to observe this interesting topological phase transition would be fascinating developments.

Acknowledgments. We acknowledge support from NSF-DMR Grant No. 1508325, the Saudi Arabian Cultural Mission to the United States for a Graduate Scholarship, and the hospitality of the Aspen Center for Physics, supported by NSF-PHY Grant No. 1066293. M.M.A. acknowledges support from NSF Grant No. DMR-1410741 and NSF Grant No. DMR-1151717.

[1] A. H. Castro Neto, F. Guinea, N. M. R. Peres, K. S. Novoselov, and A. K. Geim, Rev. Mod. Phys. **81**, 109 (2009).
[2] C. L. Kane and E. J. Mele, Phys. Rev. Lett. **95**, 226801 (2005).
[3] M. Gmitra, S. Konschuh, C. Ertler, C. Ambrosch-Draxl, and J. Fabian, Phys. Rev. B **80**, 235431 (2009).
[4] D. Pesin and A. H. MacDonald, Nature Mater. **11**, 409 (2012).
[5] A. Avsar, J. H. Lee, G. K. W. Koon, and B. Özyilmaz, 2D Mater. **2**, 044009 (2015).
[6] C. Weeks, J. Hu, J. Alicea, M. Franz, and R. Wu, Phys. Rev. X **1**, 021001 (2011).
[7] G. Giovannetti, M. Capone, J. van den Brink, and C. Ortix, Phys. Rev. B **91**, 121417 (2015).
[8] D. Marchenko, A. Varykhalov, M. Scholz, G. Bihlmayer, E. Rashba, A. Rybkin, A. Shikin, and O. Rader, Nat. Commun. **3**, 1232 (2012).
[9] E. J. Mele, J. Phys. D: Appl. Phys. **45**, 154004 (2012).
[10] D. Weckbecker, S. Shallcross, M. Fleischmann, N. Ray, S. Sharma, and O. Pankratov, Phys. Rev. B **93**, 035452 (2016).
[11] R. Bistritzer and A. H. MacDonald, Proc. Natl. Acad. Sci. USA **108**, 12233 (2011)..
[12] J. Xue, J. Sanchez-Yamagishi, D. Bulmash, P. Jacquod, A. Deshpande, K. Watanabe, T. Taniguchi, P. Jarillo-Herrero, and B. J. LeRoy, Nat. Mater. **10**, 282 (2011).
[13] P. Moon and M. Koshino, Phys. Rev. B **90**, 155406 (2014).
[14] E. McCann and M. Koshino, Rep. Prog. Phys **76**, 056503 (2013).
[15] Y. Ren, X. Deng, Z. Qiao, C. Li, J. Jung, C. Zeng, Z. Zhang, and Q. Niu, Phys. Rev. B **91**, 245415 (2015).
[16] R. Gorbachev, J. Song, G. Yu, A. Kretinin, F. Withers, Y. Cao, A. Mishchenko, I. Grigorieva, K. Novoselov, L. Levitov, and A. K. Geim, Science **346**, 448 (2014).
[17] K. Hermann, J. Phys.: Condens. Matter **24**, 314210 (2012).
[18] J. Zhang, C. Triola, and E. Rossi, Phys. Rev. Lett. **112**, 096802 (2014).
[19] A. K. Geim and I. V. Grigorieva, Nature (London) **499**, 419 (2013).
[20] J.-W. Jiang, Front. Phys. **10**, 287 (2015).
[21] M. Gmitra, D. Kochan, P. Högl, and J. Fabian, Phys. Rev. B **93**, 155104 (2016).
[22] Z. Wang, D.-K. Ki, H. Chen, H. Berger, A. H. MacDonald, and A. F. Morpurgo, Nat. Commun. **6**, 8339 (2015).
[23] M. Gmitra and J. Fabian, Phys. Rev. B **92**, 155403 (2015).
[24] D. Xiao, G.-B. Liu, W. Feng, X. Xu, and W. Yao, Phys. Rev. Lett. **108**, 196802 (2012).
[25] G.-B. Liu, W.-Y. Shan, Y. Yao, W. Yao, and D. Xiao, Phys. Rev. B **88**, 085433 (2013).
[26] F. Rose, M. O. Goerbig, and F. Piéchon, Phys. Rev. B **88**, 125438 (2013).
[27] C.-P. Lu, G. Li, K. Watanabe, T. Taniguchi, and E. Y. Andrei, Phys. Rev. Lett. **113**, 156804 (2014).
[28] A. Avsar, J. Y. Tan, T. Taychatanapat, J. Balakrishnan, G. Koon, Y. Yeo, J. Lahiri, A. Carvalho, A. Rodin, E. O'Farrell, G. Eda, A. Castro Neto, and B. Özyilmaz, Nat. Commun. **5**, 4875 (2014).
[29] D. Pierucci, H. Henck, J. Avila, A. Balan, C. H. Naylor, G. Patriarche, Y. J. Dappe, M. G. Silly, F. Sirotti, A. T. C. Johnson, M. C. Asensio, and A. Ouerghi, Nano Lett. **16**, 4054 (2016).
[30] S. Larentis, J. R. Tolsma, B. Fallahazad, D. C. Dillen, K. Kim, A. H. MacDonald, and E. Tutuc, Nano Lett. **14**, 2039 (2014).
[31] M. M. Asmar and S. E. Ulloa, Phys. Rev. Lett. **112**, 136602 (2014).
[32] M. M. Asmar and S. E. Ulloa, Phys. Rev. B **91**, 165407 (2015).
[33] D. Xiao, M.-C. Chang, and Q. Niu, Rev. Mod. Phys. **82**, 1959 (2010).
[34] Z. Qiao, X. Li, W.-K. Tse, H. Jiang, Y. Yao, and Q. Niu, Phys. Rev. B **87**, 125405 (2013).
[35] N. Hao, P. Zhang, Z. Wang, W. Zhang, and Y. Wang, Phys. Rev. B **78**, 075438 (2008).
[36] J. Li, I. Martin, M. Büttiker, and A. F. Morpurgo, Nat. Phys. **7**, 38 (2011).
[37] C. Segarra, J. Planelles, and S. E. Ulloa, Phys. Rev. B **93**, 085312 (2016).
[38] Z. Qiao, H. Jiang, X. Li, Y. Yao, and Q. Niu, Phys. Rev. B **85**, 115439 (2012).
[39] See Supplemental Material at http://link.aps.org/supplemental/10.1103/PhysRevB.94.241106 for details about calculations, TMD models, and other information.
[40] S. Konschuh, M. Gmitra, and J. Fabian, Phys. Rev. B **82**, 245412 (2010).
[41] We have kept t_R constant in the tight-binding calculations, although a gate voltage dependence is likely. This would be expected to reduce the gate voltage required to close the gap and to enlarge it in the inverted mass regime.
[42] Increasing interlayer coupling values and/or t_R by a factor of 5 enhances our estimated topological gap in the inverted mass regime to a few meV, more readily accessible in experiments.